International Journal of Heat and Mass Transfer 127 (2018) 1014–1022

Contents lists available at ScienceDirect

International Journal of Heat and Mass Transfer

journal homepage: www.elsevier.com/locate/ijhmt

# A hybrid phonon Monte Carlo-diffusion method for ballistic-diffusive heat conduction in nano- and micro- structures

Han-Ling Li (李含灵), Yu-Chao Hua (华钰超), Bing-Yang Cao (曹炳阳)*

*Key Laboratory for Thermal Science and Power Engineering of Ministry of Education, Department of Engineering Mechanics, Tsinghua University, Beijing 100084, China*

ARTICLE INFO

*Article history:*
Received 24 February 2018
Received in revised form 9 May 2018
Accepted 16 June 2018

*Keywords:*
Hybrid method
Phonon Monte Carlo
Diffusion equation
Ballistic-diffusive heat conduction

ABSTRACT

The existing phonon Monte Carlo (MC) for ballistic-diffusive heat conduction are limited to small and simple structures owing to the huge time cost following with the increasing scale. This article presents a new hybrid phonon Monte Carlo-diffusion method for ballistic-diffusive heat conduction, which successfully characterizes the ballistic effect with significantly reducing the computational cost. Based on the idea that the phonon-boundary scattering mainly affects the regions adjacent to the boundaries when the system is considerably large, the whole system is divided into three zones: the boundary MC zone and the middle diffusion zone, between which is the overlap zone. By using an alternating method and setting virtual phonon bath or specular reflection as the boundary condition for the MC zones, the results of the phonon tracing MC and diffusion equation can be coupled and converge at the overlap zone. To verify, the cross-plane and in-plane film heat conduction, where slip boundary conditions are the major characteristics of the ballistic-diffusive regime, are simulated by the hybrid method as well as standard phonon tracing MC which works as a benchmark. It is found that the hybrid method can accurately predict the distributions of temperature and heat flux in the system with nearly the same precision as the phonon tracing MC while the computation time can reduce up to 90%, validating its potential use for larger and more complex structures.



## 1. Introduction

Thermal management is of critical importance for further miniaturization and integration of the next-generation electronic devices since the danger of overheating has emerged as a major concern in the design and operation of computing devices [1]. Local hot spots, which have much higher temperature than the average value of the die, reduce the lifetime of electronic devices remarkably. According to the data reported in 2006, more than 50% of integrated circuit (IC) failures are related to thermal issues [2], and the figure is supposed to be higher now as chips are more complex boasting larger number of transistors. Therefore, it is necessary to perform the thermal analyses of electronic devices for the improving designs aimed to eliminate hot spots.

Heat conduction in micro- and nano- electronic devices is a principle path of cooling and has attracted much attention. The classical Fourier's law, which considers heat is conducted diffusively with the thermal conductivity of bulk materials, is found to be only valid in macroscale. When the characteristic length of the structure reduces to micrometer and nanometer, a growing number of experimental measurements have observed the reduction of the thermal conductivity compared to the bulk value [3–10], indicating the failure of Fourier's law. Thus, great efforts have been devoted to investigating such non-Fourier heat conduction in the micro- and nano- scale in past decades. Theoretical models which could take the memory, non-local and nonlinear effect into consideration were proposed to modify Fourier's law [11–16]. These models have explained the major contributions to non-Fourier heat conduction well, but such analyses required a considerable amount of tedious mathematical derivations even for one-dimensional systems. It is nearly unachievable to establish the closed-formed expressions in theory to predict thermal properties when considering more dimensions and more complicated structural configuration. As a result, numerical methods were extensively developed to overcome the bottleneck by converting the difficulty of analyses to computation. First-principles calculation [17] is an atomic level approach and usually works as a preprocess to obtain key parameters for other numerical methods, such as, the potential function or atomic force constant. Molecular dynamics (MD) simulation [18] directly simulates the movement of a molecular system with the achievable maximum particle number of several million and is almost limited to the scale of tens of nanometers [19]. At a larger length scale, numerically solving

* Corresponding author.
*E-mail address:* caoby@tsinghua.edu.cn (B.-Y. Cao).

https://doi.org/10.1016/j.ijheatmasstransfer.2018.06.080
0017-9310/

phonon Boltzmann transport equation (BTE) is an active topic. Phonons, which represent the quantization of lattice vibration, are deemed to be the dominating heat carriers in semiconductors [20]. Spherical harmonic method [21], lattice Boltzmann method (LBM) [22] and Monte Carlo (MC) [23–35] are the commonly used numerical solutions of BTE. Spherical harmonic method is an approximate method, whose accuracy strongly depends on the approximation order. LBM is easy to deal with complicated structures, but it is limited by the grid model and can lose some details during the solving process. The MC method is especially flexible for use with complex geometric configurations and can readily include different scattering mechanisms. To explicitly study the non-Fourier heat conduction, phonon MC simulation is a worth recommending approach.

In general, two kinds of phonon MC methods are mostly adopted in related researches: (1) direct simulation Monte Carlo (DSMC), which is also called the ensemble MC [23–25], and (2) the phonon tracing MC [26–35]. DSMC, where the trajectories of phonons are simulated simultaneously at each time step, was first introduced by Peterson for phonon transport in a Debye crystal [23] and subsequently improved via considering the dispersion and polarization [24], as well as the contribution from optical phonons [25]. In contrast, the phonon tracing MC simulates phonon trajectories independently, bringing about a significant reduction of calculation costs compared to DSMC [26]. Klitsner et al. [27] employed the phonon tracing MC to study phonon surface scattering of silicon crystals under 100 K. Then, this method is more likely to be used for room temperature simulations with a wide range of structures, including nanofilms [28], nanowires [29], nanoporous materials [30] and nanomeshes [31], as well as transistors [32]. These work have proved that the results of the phonon tracing MC have a good agreement with existing models and experiments. Recently, Tang et al. [33–35] investigated the thermal wave effects in ballistic-diffusive regime using the phonon tracing MC. To sum up, the phonon tracing MC has a very good performance for problems of the complicated geometry and multi-scattering events, and can also handle the ultrafast transport processes.

The phonon tracing MC has demonstrated that the size effect of effective thermal conductivity observed in micro- and nano- scale experiments can be explained by phonon ballistic-diffusive heat conduction, since the calculated effective thermal conductivity agrees well with experiment measurements [28,29,36]. The Knudsen number which describes the strength of the size effect is defined as $Kn = l_{MFP}/L$, where $l_{MFP}$ denotes the phonon mean-free-path (MFP) and $L$ denotes the characteristic length of the system. For the acoustic thick limit ($Kn \to 0$), the phonon–phonon scattering is sufficient and all phonons travel diffusively, as a result of which Fourier's law is valid. For the acoustic thin limit ($Kn \to \infty$), the phonon-boundary scattering dominates the transport process and phonon travels directly from one boundary to the other without scattering, resulting in the ballistic transport. For a middle $Kn$, the corresponding regime is called the ballistic-diffusive heat conduction [37]. As the physical and ubiquitous features of the boundary-driven steady state non-Fourier heat conduction, the boundary temperature jump and heat flux slip have been substantially investigated. Figs. 1 and 2 show the boundary temperature jump and boundary heat flux slip observed in the cross-plane and in-plane heat conduction in a nanofilm, respectively. The

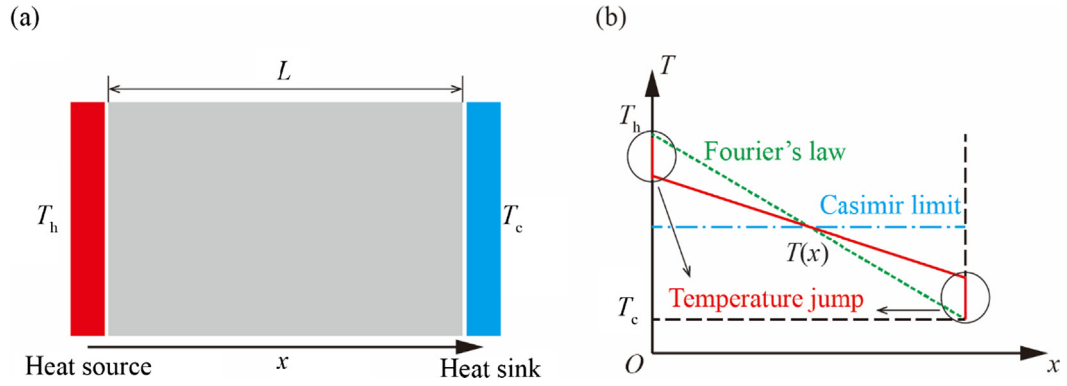


**Fig. 1.** (a) Schematic diagram of the cross-plane heat conduction in a film: a nanofilm with a characteristic length of $L$, in contact with two phonon baths of temperature $T_h$ and $T_c$. (b) Temperature jumps, $\delta T_h$ and $\delta T_c$, occur at the boundaries, but the temperature distribution is still linear in the middle region.

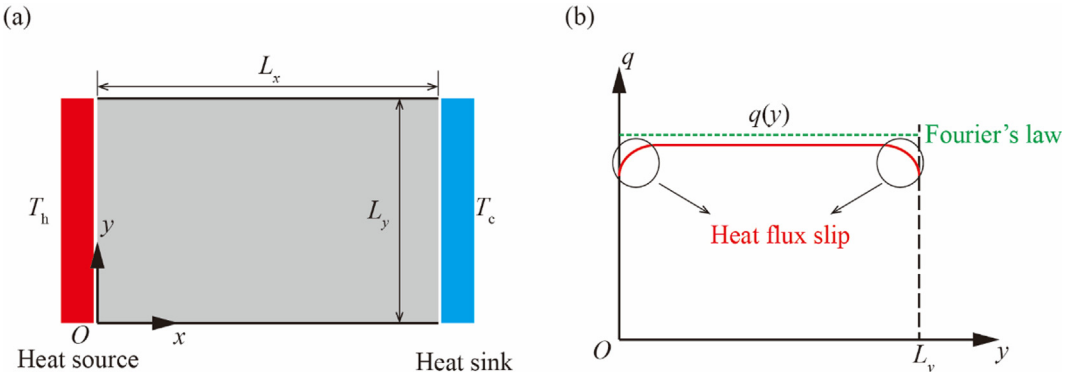


**Fig. 2.** (a) Schematic diagram of the in-plane heat conduction in a film: a nanofilm with the $x$-directional length of $L_x$ and $y$-directional thickness of $L_y$. Two phonon baths of temperature $T_h$ and $T_c$ are placed in the $x$-direction, and two adiabatic boundaries are set in the $y$-direction. (b) The heat flux slip occurs at regions adjacent to the boundaries, but $q(y)$ is nearly uniform in the middle region.

boundary temperature jump shows there is a difference between the boundary temperature and the phonon bath temperature. Aoki and Kusnezov [38] considered the boundary temperature jump to be proportional to the MFP at the corresponding temperature. The same equation was adopted by Lepri et al. [39]. Models predicting the boundary temperature jump have been well established for the films based on different approaches [28,40,41]. The boundary heat flux slip mentioned in this paper refers to the heat flux reduction observed near the lateral boundaries, in contrary to the uniform distribution predicted by Fourier's law [42]. It should not be confused with the slip boundary condition appears in phonon hydrodynamics [43], which is similar to the velocity slip condition of the rarefied gases on the solid walls. In ballistic-diffusive regime, an intriguing find is that when *Kn* is not too large, the phonon-boundary scattering only affects zones near to the boundary, and the middle region could be protected from the boundary influence and still follows Fourier's law, as shown in Figs. 1(b) and 2(b). It inspires us to develop a hybrid phonon Monte Carlo-diffusion method which employs phonon tracing MC only in the small regions near to the boundaries while the remaining ones are characterized by Fourier's law. By introducing Fourier's law which is easier and faster to solve, the new method is supposed to give a further improvement of efficiency for the phonon tracing MC, and could be applied to larger and more complicated structures where existing MC method is inefficient and hard to use. It is noted that such coupling of microscopic and macroscopic methods has been successfully developed for molecules in flow field [44] and photons in heat radiation [45], but there are few reports about the hybrid phonon MC-diffusion method.

In the present work, a hybrid phonon Monte Carlo-diffusion method which has both favorable accuracy and high efficiency is proposed. The hybrid method divides the whole system into three zones, including an overlap zone between the MC and diffusion zone. The virtual phonon bath or specular reflection is chosen as the boundary condition for the MC zones, and an alternating method is adopted to couple the phonon tracing MC and Fourier's law. More importantly, compared with the standard phonon tracing MC, the new hybrid method precisely captures the microscopic characteristics of slip boundary conditions for phonon ballistic-diffusive heat conduction in large-scale nanofilms, while improving the efficiency remarkably as the computation time can be reduced up to 10% of the phonon tracing MC.

## 2. Hybrid method

The thermal conductivity in non-metallic crystalline materials actually results from cumulative contributions of phonons that have a broad range of MFPs [46], and phonons with different frequency could have different transport regimes in the same nanostructure [47,48]. When considering the phonon spectra, phonon transport must be described by MFP spectra, which complicates the hybrid Monte Carlo-diffusion method. In this case, the lengths of the MC zones can be determined by a maximum value of the phonon MFPs in theory, and the effect of phonon spectra can be taken into consideration by redetermining the MFP of each phonon bundle after phonon–phonon scattering [24] in the MC zones. For a considerable large system, Fourier's law is still reasonable to be used for the middle zone. In this paper, since our major concern is how to describe the influence of the boundary more efficiently than existing phonon MC method, a representative MFP is adopted to validate our inspiration of coupling phonon MC and diffusion equation. Besides, the good agreements between the predicted results and experimental measurements have established the use of a proper and representative MFP as an effective simplification [3,6,10,13,29,49–51].

### 2.1. Demarcation scheme

A schematic diagram of the hybrid phonon MC-diffusion method is shown in Fig. 3, where Ω denotes the divided zone and Γ denotes the virtual boundary. The whole system is symmetrically divided into MC zones which cover the real boundaries, middle diffusion zone and overlap zones where the coupling is done. The length of the MC zone, diffusion zone and overlap zone are $L_{MC}$, $L_D$ and $L_O$, respectively. Their appropriate selections will be discussed in this part. For the convenience, all lengths discussed in the paper are nondimensionalized as the acoustic length, which is defined as $L^* = L/l_{MFP}$.

To achieve the hybrid method, one must determine the sphere of influence for the phonon-boundary scattering, so that the value of $L^*_{MC}$ can be chosen reasonably. On the one hand, $L^*_{MC}$ should be larger enough so that the phonon tracing MC can reflect the interactions between phonons and real boundaries, meanwhile the existence of the virtual boundary produced by the demarcation would not bring additional errors. On the other hand, a too large value of $L^*_{MC}$ definitely results in too much computation time, making the hybrid method losing its advantage on efficiency. An optimized value of $L^*_{MC}$, which represents a compromise between increase in accuracy and decrease in efficiency, could be evaluated in theory based on the process of the phonon tracing MC. Phonons after scattering with boundaries will carry properties determined by the boundaries at first. And they are going to undergo a random drift, where the average traveling distance is expected to be the mean-free-path. Then a phonon–phonon scattering takes place, after which the phonon property is re-determined and the boundary influence would be 'forgotten', until the phonon contacts a boundary again. To completely capture the effect of the boundary, the first drift process of all phonons after emitting should be recorded, making $L^*_{MC}$ larger than 1. In addition, the virtual boundaries of the MC zones should not affect the original interactions

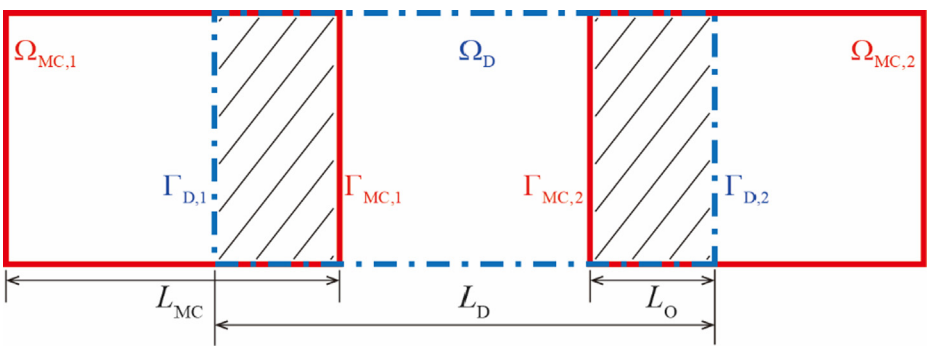


**Fig. 3.** The schematic diagram of zone dividing for the hybrid method. $L_{MC}, L_D, L_O$ is the length of the MC zone (red), diffusion zone (blue) and overlap zone (shade), respectively. (For interpretation of the references to color in this figure legend, the reader is referred to the web version of this article.)

between phonons and the real boundaries, since they actually do not exist. That is, phonons arriving at the real boundaries are not supposed to 'feel' the existence of the virtual boundaries, which can be realized as long as all phonons undergo a phonon–phonon scattering in advance and requires $L^*_{MC} \geqslant 1$, too. Considering the demand of high efficiency, it is concluded that the theoretically recommended value of $L^*_{MC}$ is 1–3, which will be verified according to the numerical results in the next section.

The value of $L^*_O$ is another numerical parameter which should be evaluated previously. Since the regions adjacent to the boundaries are strongly affected by the phonon-boundary scattering and disobey Fourier's law, the diffusion zone mustn't be near to the boundaries, which means the value of $L^*_O$ cannot be too large. However, a zero $L^*_O$ is not acceptable for the overlap zone plays a key role in accomplishing coupling, which will be discussed in detail in the next part. Based on the analyses that the sphere of influence for the phonon-boundary scattering is about one times the phonon MFP, the value of $L^*_O$ is recommended as $L^*_{MC}-1$ in theory to make sure the coupling between phonon tracing MC and Fourier's law is sufficient enough.

### 2.2. Coupling method

Here we use an alternating method, similar to the Schwarz technique proposed for the coupled Stokes/DSMC problem in the fluidic simulation [52], to couple the phonon tracing MC and Fourier's law. The basic idea of the method is to use the solution of MC/diffusion zone as the boundary condition (BC) of diffusion/MC zone in the next iteration, and the overlap zone works as an indicator of the coupling effect. A sufficient and successful coupling ought to make the phonon tracing MC and Fourier's law give the same temperature and heat flux simultaneously in the overlap region. Since Fourier's law directly relates local heat flux with local temperature gradient, the solution of the diffusion zone is always easy to do and not our concern. The key skill of the hybrid method is to set appropriate boundary conditions for the MC zone. In phonon tracing MC, there are two types of boundaries: (1) given temperature boundary which works as a phonon bath and (2) adiabatic boundary which reflects all incident phonons. Noticing that the reflecting boundary can be treated as a special non-absorbing phonon bath, we naturally set the virtual boundary of the MC zone (shown as $\Gamma_{MC}$ in Fig. 3) as a phonon bath, which immediately produces questions of how many phonons and how to emit.

In fact, the goal of the virtual phonon bath is to simulate those phonons who are emitted from the diffusion zone and will arrive at the MC zone. Considering that the heat flux at an interface is calculated by counting the net number of phonons passing through in the phonon tracing MC, the first question can be transferred to determine the heat flux, thus the net number of phonons can be given in turn. The most intuitive way is to use the solution of the diffusion zone as the value of boundary heat flux for the MC zone. Let the net number of phonons across $\Gamma_{MC}$ given by tracing MC and Fourier's law is $N_{vir,MC}$ and $N_{vir,D}$, respectively, and define $N_{vir,emit} = N_{vir,MC} - N_{vir,D}$ as the number of emitting phonons for the virtual phonon bath. A positive $N_{vir,emit}$ means the virtual phonon bath has absorbed more phonons than the prediction from the diffusion equation, and these extra absorbed phonons should reemit at the virtual phonon bath, travel in the MC zone until absorbed by the real bath, as a result of which the temperature of $\Gamma_D$ will be higher. Thus, Fourier's law predicts a higher heat flux at $\Gamma_{MC}$ and increases $N_{vir,D}$, reducing $N_{vir,emit}$ to zero. For a negative $N_{vir,emit}$, although phonons emitted from the virtual bath bring a decrease in temperature and $N_{vir,D}$ conversely, $N_{vir,emit}$ still converges to zero. A special case that $N_{vir,D} = 0$ is worth noting, which means the boundary heat flux of the MC zone and the net number of phonons across $\Gamma_{MC}$ should be zero. In this case, the virtual boundary works as a total reflection boundary for the phonon tracing MC and $N_{vir,MC}$ is naturally zero, which satisfies $N_{vir,emit} = 0$, too. To sum up, the alternating method could guarantee that the phonon tracing MC and Fourier's law result in an equal heat flux at $\Gamma_{MC}$.

As for the question of how to emit, simply copy the emitting means of a real boundary will certainly be wrong since it is contrary to the physical reality that there is no phonon bath actually, which can be explained by the different means of boundary and internal emitting in further. According to the Ref. [28], phonon intensity emitting from a black-body boundary is characterized as

$$E_b = \sigma_p T_b^4 \tag{1}$$

in which the parameter $\sigma_p$ is known as the phonon Stephen Boltzmann constant, $T_b$ denotes the boundary temperature. For phonons emitting from a unit volume in the media, the intensity is

$$dQ = 4\varepsilon\sigma_p T^4 dV \tag{2}$$

where $\varepsilon$ is the phonon emissivity ($\varepsilon = l^{-1}_{MFP}$), $T$ is the local temperature and can be calculated based on the local thermal equilibrium assumption. Although Eq. (1) is significantly different from Eq. (2), it has been found that placing the location of the virtual phonon bath further into the diffusion zone by a shifting distance of $L_S$ can overcome the irrationality caused by directly using Eq. (1). In this way, phonons emitting from the virtual phonon bath will travel a distance and undergo phonon–phonon scattering before entering into the MC zone. Based on the analyses of $L^*_{MC}$, it is supposed that the effect of the virtual boundary can be eliminated and phonons arriving at the MC zone will 'look' like emitted from the diffusion zone, as long as $L^*_S \geqslant 1$. Actually, it means the simulated length for the phonon tracing MC is $L_{MC} + L_S$ in the iteration, but only the results in the MC zone with a length of $L_{MC}$ is valid and recorded. The additional length of $L_S$ just works as a preconditioner to make sure the temperature of the MC zone can be calculated correctly and be equal to the solution of Fourier's law in the overlap zone.

Although the coupling process only initiatively guarantees the equivalence of heat flux at $\Gamma_{MC}$, it is expected to achieve the equivalence of both temperature and heat flux in the whole overlap zone with reasonable zone length, which will be verified by the numerical results. The overlap zone is essential for the hybrid method, without which the coupling effect cannot be assessed.

### 2.3. Procedure of the hybrid method

Based on the above ideas, Fig. 4 illustrates the algorithm of the hybrid MC-diffusion method, which has the following procedures: **(1) Initialization:** Predict a temperature and heat flux distribution of the whole system to start the iteration. Solution of Fourier's law is recommended as a good choice. **(2) Phonon tracing MC**: Update the iteration number and alternate the boundary heat flux of the MC zone by the diffusion solution of the last iteration. Virtual phonon bath with a shifting length is introduced to absorb phonons emitted from the real boundary and reemit excess phonons with a number of $N_{vir,emit}$. **(3) Diffusion solution**: Alternate the boundary temperature of the diffusion zone by the results of MC zone and get diffusive solution of the heat flux in this iteration by Fourier's law. **(4) Stop checking**: If the heat flux of the phonon tracing MC and Fourier's law converge to equality, end the iteration and output results. Otherwise it proceeds to (2) and repeats.

## 3. Simulation results

In this section, the cross-plane and in-plane heat conduction in films, as shown in Figs. 1 and 2, are simulated by the new hybrid

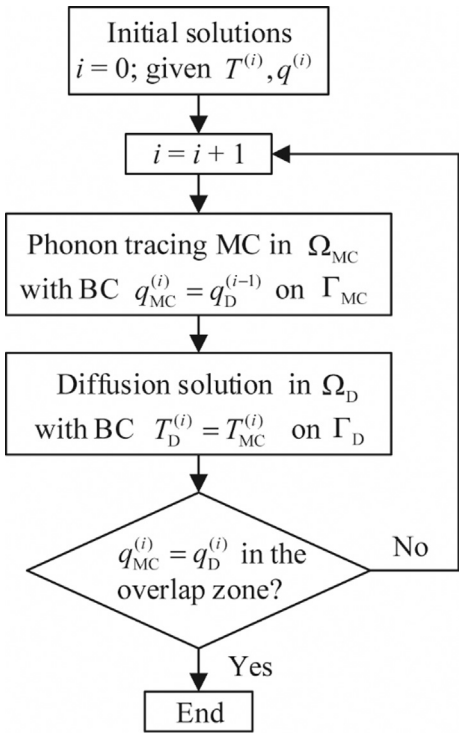


**Fig. 4.** Algorithm of the coupling process in the hybrid method.

MC-diffusion method respectively. The two cases are chosen not only for the fact that they can exhibit the effect of phonon-boundary scattering well, but also considering the feasibility of using the phonon tracing MC as a benchmark. The Debye theory are adopted in the calculation, and only phonon–phonon scattering and phonon-boundary scattering are taken into consideration. These simplifications including the gray-media approximation don't affect the comparisons of the hybrid method and standard phonon tracing MC. All results are in steady-state. Simulations are carried out on a computer with an Intel(R) Core(TM) i7-4790 CPU of 3.60 GHz and 32.0 GB RAM. To avoid the random error of the results, the total number of phonon bundles is $N = 2 \times 10^6$ for the cross-plane film conduction. For the in-plane case, $10^7$ phonon bundles is needed for every MFP of the thickness, which means $N = \frac{L_y}{l_{MFP}} \times 10^7$.

### 3.1. Cross-plane heat conduction in films

#### 3.1.1. Numerical parameters

It is necessary to discuss the specific values of the numerical parameters used in demarcation at first. For the cross-plane case, as depicted in Fig. 1(b), the influence range of the phonon-boundary scattering for the temperature profile is exactly limited to the boundaries, while the rest of the system still follows Fourier's law. In fact, the input temperature difference, $\Delta T = T_1 - T_2$, can be decomposed into the two boundary jumps, $\delta T_1$, $\delta T_2$, and the gradient contribution: $\Delta T = \delta T_1 + \delta T_2 + \int \nabla T \cdot dx$ [38]. After using the boundary temperature jump conditions, theoretical models based on diffusion equation successfully predicted the temperature distributions [28,40,41]. In this way, the length of the MC zone can be smaller than MFP, as long as the boundary temperature jump can be accurately simulated, and the length of the diffusion zone can be close to the length of the entire system. As a validation, it is found that the temperature results of the hybrid MC (HM) and hybrid diffusion solution (HD) always agree well at the overlap zones for $L_{MC}^* = 0.5$, 1.0, 1.5, 2.0 and $L_O^* = 1.9$, 1.5, 1.0, 0.5 at $Kn = 0.1$ (not reported here). Besides, it is noted that results of $L_S^* < 1$ do not satisfy the equivalence of temperature at the overlap zones as expected. Although the constraints on these zone dividing parameters mentioned in Section 2.1 can be relaxed for the cross-plane case, their values are set as $L_{MC}^* = 2$, $L_O^* = 1$ and $L_S^* = 1$ in following simulation for the sake of conservation.

#### 3.1.2. Results and discussions

After determining the zone dividing parameters, the temperature results of the new hybrid method for different film lengths are illustrated in Fig. 5. For the convenience of comparison, the $x$-axis is defined as $X = x/L$, and the temperature is been nondimensionalized as $T^* = \frac{(T-T_c)}{(T_h-T_c)}$, both resulting in a range of 0 to 1. The temperature equality of the HM and HD at the overlap zones is clearly demonstrated by the insets, and the hybrid method has a good agreement with standard phonon tracing MC simulation for different Knudsen numbers. For $Kn = 0.01$, the film is so long that all phonons travel diffusively, making the boundary temperature jump negligible and the temperature distribution similar to the prediction of Fourier's law. However, as $Kn$ increases, ballistic effect plays a more and more important role and the temperature jump is not negligible any more, as shown in Figs. 7(b)–(d). For these cases, Fourier's law fails and the hybrid method is proved to have a good performance. When $Kn$ is more than 0.2, the film length is small enough to directly use the phonon tracing MC and the hybrid method loses its value of application. In this way, the valuable application range of the hybrid phonon MC-diffusion method is defined as $Kn \leqslant 0.2$.

To better reveal the accuracy of the hybrid method, the values of boundary temperature jump for different $Kn$ are calculated by the hybrid method and phonon tracing MC. Fig. 6 shows the results at 300 K, where boundary temperatures are set as $T_h = 305$ K and $T_c = 295$ K. The hybrid method has a good consistency with the standard phonon tracing MC and theoretical models as expected. Besides, we also calculate the dimensionless effective thermal conductivity, as illustrated in Table 1. The relative deviation of the thermal conductivity increases as $Kn$, as the phonon-boundary scattering plays a more important role and the employment of Fourier's law gradually fails to describe the middle region. However, the maximum value of thermal conductivity relative deviation is about 0.3% for $Kn \leqslant 0.2$, verifying that the hybrid method has same precision with standard phonon tracing MC quantitatively.

Table 1 also gives the results of the computation times. It can be seen that the hybrid method has a much better efficiency compared to standard phonon tracing MC without causing significant deviation, as the computation time can be reduced by up to 90%. The phonon tracing MC could be an efficient method when $Kn$ is large, as its computation time greatly decreases with $Kn$. For the hybrid method, since the main time-consuming process is the MC simulation, the computation time is expected to be a constant when the length of the MC zone is fixed, which is verified by the results of $Kn \leqslant 0.1$ in Table 1. The increasing computational cost for $Kn > 0.1$ is caused by more number of iteration, and it may be even more than the time of the standard phonon tracing MC, which suggests there is no need to use the hybrid method for $Kn > 0.2$.

### 3.2. In-plane heat conduction in films

#### 3.2.1. Numerical parameters

The major concern of the in-plane heat conduction is the boundary heat flux slip caused by the interactions between phonons and the lateral adiabatic walls (shown as the black bold lines

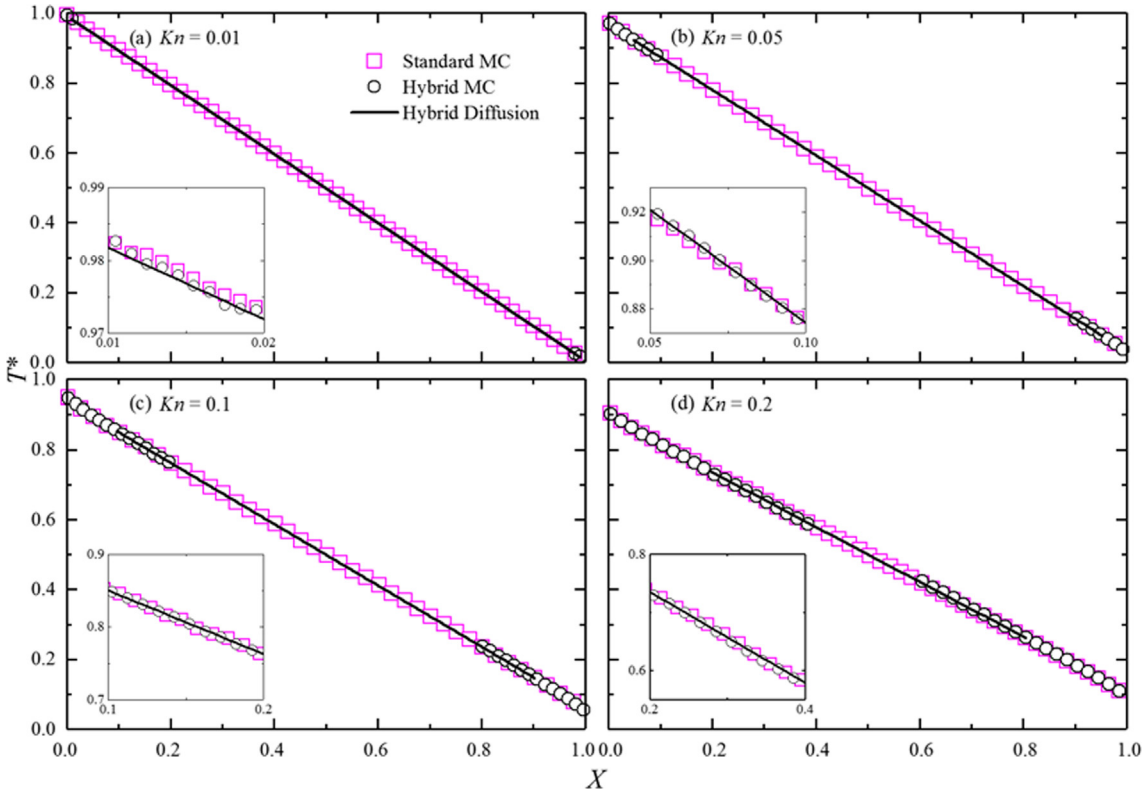


**Fig. 5.** Cross-plane temperature distribution varying with *Kn*. Insets show the enlarged figure of the temperature distribution at the left overlap zone.

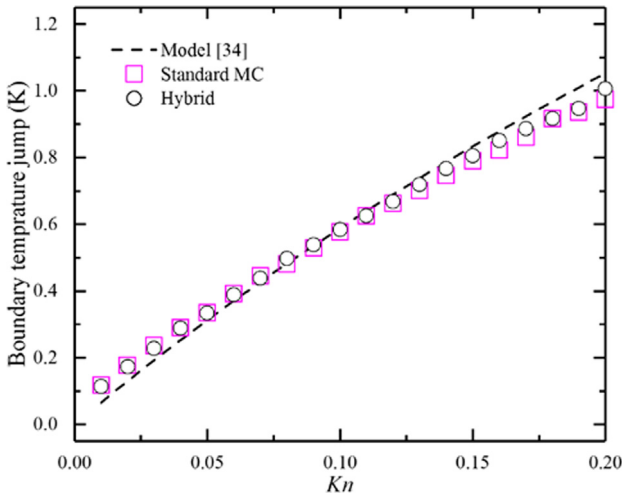


**Fig. 6.** Cross-plane boundary temperature jump varying with *Kn*. The theoretical model of the boundary temperature jump [28] is still illustrated.

in Fig. 2(a)), so the system is divided in the *y*-direction and the Knudsen number is defined as $Kn = l_{MFP}/L_y$. The lateral boundary conditions are set as total diffusive reflection to generate an outstanding boundary heat flux slip [42], and the value of $L_x^*$ is set as 100 to eliminate the *x*-directional size effect. The influence of the zone dividing parameters on calculated heat flux distribution is shown in Fig. 7 for $Kn = 0.1$, where only the lower half of the symmetrical film is drawn. The heat flux distribution along *x*-direction is nondimensionalized as $q_x^*(y) = q_x(y)/q_{x,F}$, in which $q_{x,F}$ is the result of Fourier's law and independent of *y* owing to the adiabatic boundaries. $q(y)$ calculated by diffusion equation is a straight line at the diffusion zones, as the vertical lines illustrated in Fig. 7. As a result, $N_{vir,D}$ at $\Gamma_{MC}$ equals to zero, and the virtual phonon bath becomes a reflection boundary. The total specular reflection condition, $p_{virtual} = 1$, is employed, which means the virtual reflection boundary has no resistance on the phonon transport.

On the one hand, Fig. 7 demonstrates that when $L_{MC}^*$ is too small to cover all locations where the heat flux slip occurs, the heat flux distribution obtained by HM still varies with $L_{MC}^*$. Increasing $L_{MC}^*$ greatly optimizes the convergence, which is deemed to be realized at $L_{MC}^* = 3$, for it has little difference with the results of $L_{MC}^* = 4$. To give a quantitative criterion for the value of $L_{MC}^*$, locations with a

**Table 1**
The effective thermal conductivity and computation time for the cross-plane heat conduction.

| | *Kn* | 0.01 | 0.02 | 0.05 | 0.1 | 0.15 | 0.2 |
|---|---|---|---|---|---|---|---|
| $k_{eff}/k_{bulk}$ | MC | 0.986 | 0.975 | 0.937 | 0.874 | 0.825 | 0.778 |
| | Hybrid | 0.987 | 0.975 | 0.938 | 0.876 | 0.826 | 0.780 |
| | $\frac{\lvert k_{Hybrid}-k_{MC}\rvert}{k_{MC}}$ (%) | 0.1 | 0.0 | 0.1 | 0.2 | 0.1 | 0.3 |
| Computation time | MC (s) | 58.7 | 29.5 | 12.0 | 6.4 | 4.2 | 3.9 |
| | Hybrid (s) | 4.9 | 4.9 | 4.9 | 5.1 | 5.4 | 6.0 |
| | $\frac{t_{Hybrid}}{t_{MC}}$ (%) | 8.4 | 16.6 | 40.8 | 79.7 | 128.6 | 153.9 |

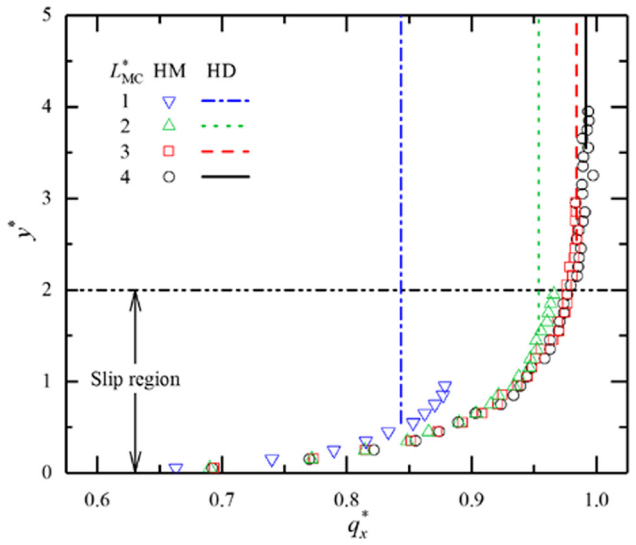


**Fig. 7.** The effect of $L_{MC}$ on the heat flux distribution in the lower half of the film. $Kn = 0.1$ and other length parameters are fixed as $L^*_O = 0.5$, $L^*_S = 0$. HM and HD are the abbreviations of the hybrid Monte Carlo and hybrid diffusion, respectively.

dimensionless heat flux smaller than 0.98 are defined as the slip region, which approximately covers a length of two times the phonon MFP according the converged results. On the other hand, since diffusion equation is impossible to get a curved heat flux profile under the adiabatic condition, the equality of the heat flux distribution at the overlap zone is definitely to fail when the diffusion zone is too close to the adiabatic walls, shown as the dash-dotted and dotted lines in Fig. 7. More importantly, the total specular reflection boundary itself has been accurate enough to simulate the phonons who are emitted from the diffusion zone and arrive at the MC zones, making there is no need to introduce a shift length of $L_S$. As a summary, the zone dividing parameters are defined as $L^*_{MC} \geqslant 2$, $L^*_O \leqslant L^*_{MC} - 2$, $p_{virtual} = 1$, and $L^*_S = 0$.

### 3.2.2. Results and discussions

The heat flux distributions of the hybrid method and the benchmark MC for different film thicknesses are shown in Fig. 8. The dimensionless $y$ coordinate is $Y = y/L_y$, and the theoretical model [42] based on analytically solving BTE under the condition of $L_x \to \infty$ is also illustrated in Fig. 8. Although the zone dividing parameters are different for different film thicknesses, their values all meet the forementioned limitations to make sure the equality of the heat flux distribution at the overlap zone has been obtained, as the insets in Fig. 8 show. Compared to the standard phonon tracing MC and the theoretical model, the hybrid phonon MC-diffusion method has a good consistency, and accurately characterizes the boundary heat flux slip. Errors mainly appear in the diffusion zone, where the results of HD are slightly below the reference values, and the deviation increases as $Kn$. The decrement of the straight part of the heat flux distribution from Figs. 8(a) to (d) is owing to the fact that more locations are affected by the phonon-boundary interactions as $Kn$ increases. When $Kn = 0.2$, the heat flux profile completely becomes a curved line and the middle region does not follow Fourier's law any more. It is emphasized again that problems of a larger $Kn$ are not the goal of the hybrid method, and the valuable application range of the hybrid phonon MC-diffusion method is limited to $Kn \leqslant 0.2$ for the in-plane case, which is the same as the previous conclusion for the cross-plane case.

In addition, effective thermal conductivity can be calculated and its results are given in Table 2, in which different dividing parameters are chosen to get a coarse balance between accuracy and efficiency for different $Kn$. The thermal conductivity calculated by the

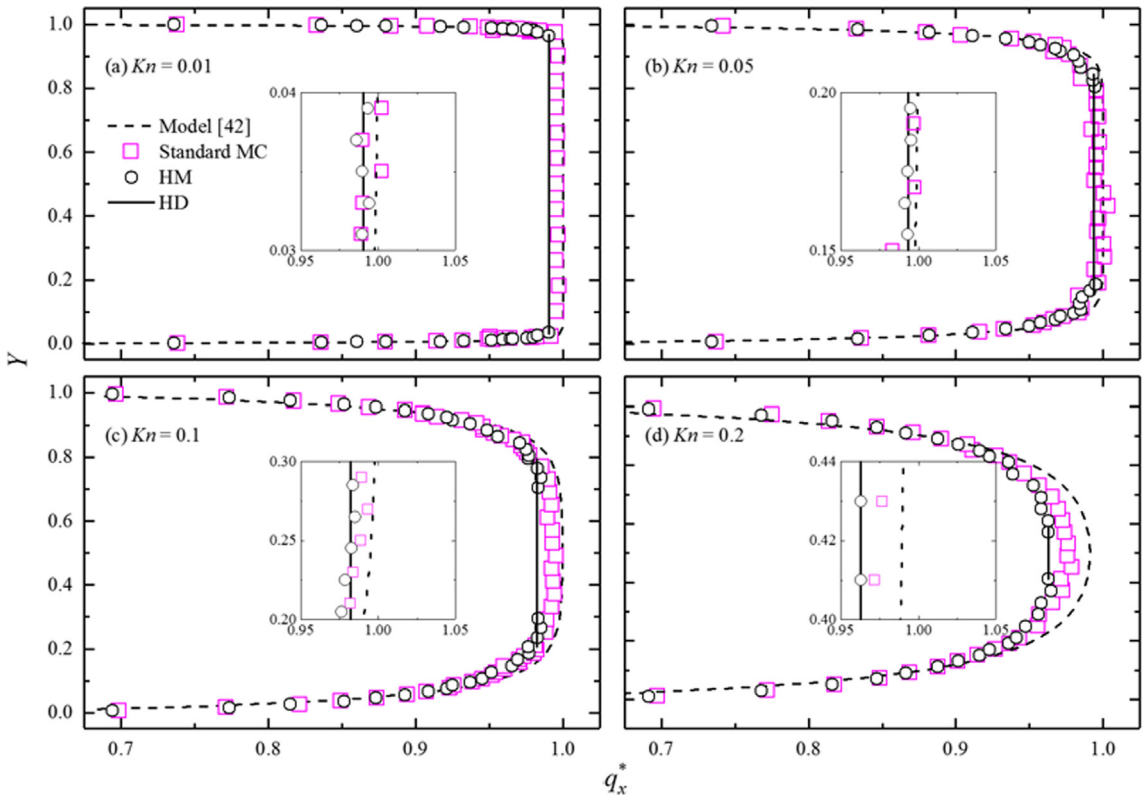


**Fig. 8.** The heat flux distribution varying with $Kn$. From (a) to (d), the values of $L^*_{MC}$ are 4, 4, 3, 2.2, and corresponding $L^*_O$ are 1, 1, 1, 0.2. The insets shows the enlarged figures of the bottom overlap zone with more nodes displayed.

**Table 2**
The effective thermal conductivity and computation time for the in-plane film conduction. Three groups of numerical parameters are used: (1) $L^*_{MC} = 4$ and $L^*_O = 1$ for $Kn$ = 0.01 and 0.05; (2) $L^*_{MC} = 3$ and $L^*_O = 1$ for $Kn$ = 0.1 and 0.15; (3) $L^*_{MC} = 2.2$ and $L^*_O = 0.2$ for $Kn$ = 0.2.

| | $Kn$ | 0.01 | 0.05 | 0.1 | 0.15 | 0.2 |
|---|---|---|---|---|---|---|
| $k_{eff}/k_{bulk}$ | Model [42] | 0.998 | 0.983 | 0.964 | 0.946 | 0.927 |
| | MC | 0.993 | 0.978 | 0.957 | 0.941 | 0.923 |
| | Hybrid | 0.982 | 0.978 | 0.956 | 0.940 | 0.921 |
| | $\frac{\lvert k_{Hybrid}-k_{MC}\rvert}{k_{MC}}$ (%) | 0.1 | 0.1 | 0.1 | 0.1 | 0.2 |
| Computation time | MC (s) | 6289 | 1276 | 663 | 448 | 332 |
| | Hybrid (s) | 281 | 281 | 219 | 219 | 142 |
| | $\frac{t_{Hybrid}}{t_{MC}}$ (%) | 4 | 22 | 33 | 49 | 42 |

hybrid method is found to be almost the same to that of the standard phonon tracing MC, with a relative error less than 0.3%. The deviation between the hybrid method and the theoretical model is a bit larger but still less than 1%, demonstrating the accuracy of the hybrid method again. More importantly, Table 2 also gives the computation times and demonstrates that the hybrid method can greatly reduce the computation time without causing significant deviation. For example, the time consumption of the hybrid method is one order of magnitude less than that of the standard MC for $Kn = 0.01$. When it comes to the maximum value of $Kn$, the hybrid method can still reduce the time cost in half thanks to the reduction of the size of MC simulation.

## 4. Conclusions

In the present work, we develop a new hybrid phonon Monte Carlo-diffusion method which can simulate large-scale structures efficiently while capturing microscopic details accurately for ballistic-diffusive heat conduction. Based on the idea that the phonon-boundary scattering mainly affects the regions near to the boundaries while phonons in the middle region still travel diffusively for a considerably large structure, the hybrid method divides the whole system into three zones: MC zone, diffusion zone and overlap zone. Phonon MC and diffusion equation (Fourier's law) are coupled by using one's results as the other's boundary conditions, and the equality of the distribution of temperature and heat flux at the overlap zone works as an indicator of successful coupling.

The hybrid method was then used to simulate cross-plane and in-plane film heat conduction. For the cross-plane case, the zone dividing parameters are recommended to be $L^*_{MC}$ =2 and $L^*_O = 1$. For the in-plane case, they are limited to $L^*_{MC} \geqslant 2$ and $L^*_O \leqslant L^*_{MC} - 2$. By using virtual phonon bath with a shifting length of $L^*_S = 1$ or specular reflection condition for the virtual boundary of the MC zone, the new hybrid method successfully acquires the boundary temperature jump and boundary heat flux slip for large scale cases ($Kn \leqslant 0.2$) of film heat conduction. For a larger $Kn$, there is no need to introduce the hybrid method since the phonon tracing MC is sufficient enough. More importantly, time cost of the new hybrid method can be reduced as much as 90% compared to that of the standard phonon tracing MC.

A more general heat conduction problem can be decomposed into two sub-problems: heat flux being perpendicular and parallel to the boundary. Since our hybrid phonon Monte Carlo-diffusion method has a great accuracy and high-efficiency for both the two sub-problems, it is supposed to be further developed to efficiently simulate the heat conduction in more complex structures, and the detailed description of the phonon frequency will be considered.

## Conflict of interest

We declare no any interest conflict.

## Acknowledgements

This work is financially supported by National Natural Science Foundation of China (No.51676108), and Science Fund for Creative Research Groups (No. 51621062).

## References

[1] S. Reda, Thermal and power characterization of real computing devices, IEEE J. Em. Sel. Top. C 1 (2011) 76–87.
[2] M. Pedram, S. Nazarian, Thermal modeling, analysis, and management in VLSI circuits: principles and methods, Proc. IEEE 94 (2006) 1487–1501.
[3] M. Asheghi, Y.K. Leung, S.S. Wong, et al., Phonon-boundary scattering in thin silicon layers, Appl. Phys. Lett. 71 (1997) 1798–1800.
[4] Y.S. Ju, K.E. Goodson, Phonon scattering in silicon films with thickness of order 100 nm, Appl. Phys. Lett. 74 (1999) 3005–3007.
[5] Y.S. Ju, K. Kurabayashi, K.E. Goodson, Thermal characterization of anisotropic thin dielectric films using harmonic Joule heating, Thin Solid Films 339 (1999) 160–164.
[6] W. Liu, M. Asheghi, Phonon-boundary scattering in ultrathin single-crystal silicon layers, Appl. Phys. Lett. 84 (2004) 3819–3821.
[7] D. Song, G. Chen, Thermal conductivity of periodic microporous silicon films, Appl. Phys. Lett. 84 (2004) 687–689.
[8] Y.S. Ju, Phonon heat transport in silicon nanostructures, Appl. Phys. Lett. 87 (2005) 153106.
[9] P.E. Hopkins, C.M. Reinke, M.F. Su, et al., Reduction in the thermal conductivity of single crystalline silicon by phononic crystal patterning, Nano Lett. 11 (2011) 107–112.
[10] A.A. Maznev, J. Cuffe, J.K. Eliason, et al., Direct measurement of room-temperature nondiffusive thermal transport over micron distances in a silicon membrane, Phys. Rev. Lett. 110 (2013) 025901.
[11] Y.Y. Guo, M.R. Wang, Phonon hydrodynamics and its applications in nanoscale heat transport, Phys. Rep. 595 (2015) 1–44.
[12] S.L. Sobolev, Local non-equilibrium transport models, Phys.–uspekhi 40 (1997) 1043–1053.
[13] F.X. Alvarez, D. Jou, Memory and nonlocal effects in heat transport: From diffusive to ballistic regimes, Appl. Phys. Lett. 90 (2007) 083109.
[14] D. Jou, G. Lebon, Extended Irreversible Thermodynamics, fourth ed., Springer, Netherlands: Dordrecht, 2010.
[15] S.L. Sobolev, Nonlocal diffusion models: Application to rapid solidification of binary mixtures, Int. J. Heat Mass Tran. 71 (2014) 295–302.
[16] S. Lee, D. Broido, K. Esfarjani, et al., Hydrodynamic phonon transport in suspended graphene, Nat. Commun. 6 (2015) 6290.
[17] K. Esfarjani, G. Chen, H.T. Stokes, Heat transport in silicon from first principles calculations, Phys. Rev. B 328 (2011) 293, 293–293.
[18] S. Maruyama, Molecular dynamics method for microscale heat transfer Chap. 6, in: W.J. Minkowycz, E.M. Sparrow (Eds.), Advances in Numerical Heat Transfer, Taylor & Francis, New York, 2000, pp. 189–226.
[19] J.A. Elliott, Novel approaches to multiscale modelling in materials science, Int. Mater. Rev. 56 (2011) 207–225.
[20] J.M. Ziman, Electrons and Phonons: The Theory of Transport Phenomena in Solids, Clarendon Press, Oxford, 2001.
[21] Z.Y. Han, N. Goldsman, M.A. Stettler, The realization of scattering matrix approach to transport modeling through spherical harmonics, Solid State Electron. 43 (1999) 493–501.
[22] A. Nabovati, D.P. Sellan, C.H. Amon, On the lattice Boltzmann method for phonon transport, J. Comput. Phys. 230 (2011) 5864–5876.
[23] R.B. Peterson, Direct simulation of phonon-mediated heat transfer in a Debye crystal, J. Heat. Trans. 116 (1994) 815–822.
[24] S. Mazumder, A. Majumdar, Monte Carlo study of phonon transport in solid thin films including dispersion and polarization, J. Heat Trans. 123 (2001) 749–759.
[25] A. Mittal, S. Mazumder, Monte Carlo study of phonon heat conduction in silicon thin films including contributions of optical phonons, J. Heat Trans. 132 (2010) 052402.

[26] J.P.M. Péraud, N.G. Hadjiconstantinou, An alternative approach to efficient simulation of micro/nanoscale phonon transport, Appl. Phys. Lett. 101 (2012) 153114.
[27] T. Klitsner, J.E. Vancleve, H.E. Fischer, et al., Phonon radiative heat transfer and surface scattering, Phys. Rev. B 38 (1988) 7576–7594.
[28] Y.C. Hua, B.Y. Cao, Phonon ballistic-diffusive heat conduction in silicon nanofilms by Monte Carlo simulations, Int. J. Heat Mass Tran. 78 (2014) 755–759.
[29] Y.C. Hua, B.Y. Cao, Ballistic-diffusive heat conduction in multiply-constrained nanostructures, Int. J. Therm. Sci. 101 (2016) 126–132.
[30] Y.C. Hua, B.Y. Cao, Anisotropic heat conduction in two-dimensional periodic silicon nanoporous films, J. Phys. Chem. C 121 (2017) 5293–5301.
[31] N.K. Ravichandran, A.J. Minnich, Coherent and incoherent thermal transport in nanomeshes, Phys. Rev. B 89 (2014) 2096–2107.
[32] J. Schleeh, J. Mateos, I. Íñiguez-de-la-Torre, et al., Phonon black-body radiation limit for heat dissipation in electronics, Nat. Mater. 14 (2014) 187–192.
[33] D.S. Tang, Y.C. Hua, B.D. Nie, et al., Phonon wave propagation in ballistic-diffusive regime, J. Appl. Phys. 119 (2016) 124301.
[34] D.S. Tang, Y.C. Hua, B.Y. Cao, Thermal wave propagation through nanofilms in ballistic-diffusive regime by Monte Carlo simulations, Int. J. Therm. Sci. 109 (2016) 81–89.
[35] D.S. Tang, B.Y. Cao, Ballistic thermal wave propagation along nanowires modeled using phonon Monte Carlo simulations, Appl. Therm. Eng. 117 (2017) 609–616.
[36] Y.C. Hua, B.Y. Cao, The effective thermal conductivity of ballistic-diffusive heat conduction in nanostructures with internal heat source, Int. J. Heat Mass Tran. 92 (2016) 995–1003.
[37] G. Chen, Ballistic-diffusive heat-conduction equations, Phys. Rev. Lett. 86 (2001) 2297–2300.
[38] K. Aoki, D. Kusnezov, Fermi-Pasta-Ulam beta model: boundary jumps, Fourier's law, and scaling, Phys. Rev. Lett. 86 (2001) 4029–4032.
[39] S. Lepri, R. Livi, A. Politi, Thermal conduction in classical low-dimensional lattices, Phys. Rep. 377 (2003) 1–80.
[40] J. Maassen, M. Lundstrom, Steady-state heat transport: Ballistic-to-diffusive with Fourier's law, J. Appl. Phys. 117 (2015) 011305.
[41] S.L. Sobolev, Discrete space-time model for heat conduction: Application to size-dependent thermal conductivity in nano-films, Int. J. Heat Mass Tran. 108 (2017) 933–939.
[42] Y.C. Hua, B.Y. Cao, Slip boundary conditions in ballistic-diffusive heat transport in nanostructures, Nanosc. Microsc. Therm. 3 (2017) 159–176.
[43] F.X. Alvarez, D. Jou, A. Sellitto, Phonon hydrodynamics and phonon-boundary scattering in nanosystems, J. Appl. Phys. 105 (2009) 014317.
[44] D.S. Watvisave, B.P. Puranik, U.V. Bhandarkar, A hybrid MD-DSMC coupling method to investigate flow characteristics of micro-devices, J. Comput. Phys. 302 (2015) 603–617.
[45] T. Hayashi, Y. Kashio, E. Okada, Hybrid Monte Carlo-diffusion method for light propagation in tissue with a low-scattering region, Appl. Optics 42 (2003) 2888–2896.
[46] J.P. Freedman, J.H. Leach, E.A. Preble, et al., Universal phonon mean free path spectra in crystalline semiconductors at high temperature, Sci. Rep.-UK 3 (2013) 2963–2968.
[47] K. Regner, D. Sellan, Z. Su, et al., Broadband phonon mean free path contributions to thermal conductivity measured using frequency domain thermoreflectance, Nat. Commun. 4 (2013) 1640–1646.
[48] T. Feng, W. Yao, Z. Wang, et al., Spectral analysis of nonequilibrium molecular dynamics: Spectral phonon temperature and local nonequilibrium in thin films and across interfaces, Phy. Rev. B 95 (2017) 195202.
[49] W. Liu, K. Etessam-Yazdani, R. Hussin, et al., Modeling and data for thermal conductivity of ultrathin single-crystal SOI layers at high temperature, IEEE T. Electron Dev. 53 (2006) 1868–1876.
[50] A. Majumdar, Microscale heat conduction in dielectric thin films, J. Heat Trans. 115 (1993) 7–16.
[51] M. Jeng, R. Yang, D. Song, et al., Modeling the thermal conductivity and phonon transport in nanoparticle composites using Monte Carlo simulation, J. Heat Trans. 130 (2008) 042410.
[52] O. Aktas, N.R. Aluru, A combined continuum/DSMC technique for multiscale analysis of microfluidic filters, J. Comput. Phys. 178 (2002) 342–372.